The changing sulphur content of a northern Chinese dust storm: initiation, attenuation and culmination

Xiaolei Feng[a], Longyi Shao[a*], Tim Jones[b], Yaowei Li[c], Mengyuan Zhang[a], Shuoyi Ge[a], Yaxin Cao[a], Kelly BeruBe[d], Daizhou Zhang[e]

[a] State Key Laboratory of Coal Resources and Safe Mining, and College of Geoscience and Surveying Engineering, China University of Mining and Technology (Beijing), Beijing 100083, China

[b] School of Earth and Environmental Sciences, Cardiff University, Park Place, Cardiff, CF10, 3YE, UK

[c] Hebei Center for Ecological and Environmental Geology Research, Hebei GEO University, Shijiazhuang, 050031, China

[d] School of Biosciences, Cardiff University, Museum Avenue, Cardiff, CF10 3AX, Wales, UK

[e] Faculty of Environmental and Symbiotic Sciences, Prefectural University of Kumamoto, Kumamoto, 62-8502, Japan

*Correspondence: ShaoL@cumtb.edu.cn

Graphical abstract

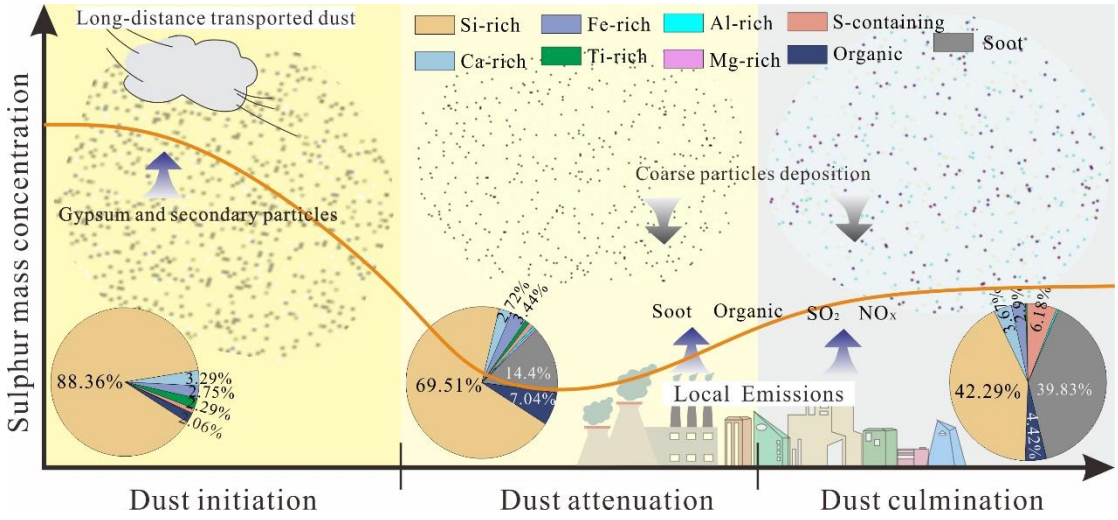

Highlights

1. The investigated dust storms have three recognisable stages: initiation, attenuation and culmination.
2. The high concentration of S in the initiation stage was provided by S containing minerals from the source area.
3. The secondary chemical reactions in the dust storm are comparable to those in haze events.

Abstract

It is predicted that changing climate trends on land in northern China will be associated with increasingly frequent and severe dust storms. These regionally extensive storms could have a serious impact on the environment and human respiratory health. A severe dust storm event hit Beijing from March 15th to 20th, 2021, and airborne particles from this dust storm episode were collected. The types, size distributions, and chemical compositions of the dust storm particles were analysed using individual

particle analysis techniques. This dust storm episode was divided into three recognisable stages, which were initiation, attenuation and culmination by the PM10 pollution levels and horizontal visibility. Field Emission Scanning Electron Microscopy coupled with an Energy-dispersive X-ray Spectrometer recorded three basic particle groups: minerals, soot, and organic particles, of which minerals were the most abundant. Over the duration of the dust storm, the relative number percentage of minerals continuously decreased, while that of soot and organic particles correspondingly increased. The dust particles were mostly distributed in the 1-2 μm size range. In the attenuation and culmination stages, the number percentage of sub-micrometer particles was higher than in the initiation stage, probably due to coarser minerals being deposited and the finer minerals formed by secondary reactions remaining airborne. In comparison to the initiation stage, the presence of anthropogenic toxic metals increased over the attenuation and culmination stages. Anthropogenic emissions, both particulate and gaseous, were mixed with the crust-derived dust, modifying the dust bulk composition and therefore changing the potential impacts of the dust storm in the later stages. The sulphur concentration was highest in the initiation stage (27.8 $\mu g/m^3$), with sulphur concentrations mainly consisting of gypsum from the source area and secondary reactions during early transport. In the attenuation and culmination stages, the overall mass concentration of sulphur decreased significantly, while the various sulphur-containing minerals increased.

Keywords

62 Airborne mineral particles; Sulphur; Secondary chemical reaction; Number-size
63 distributions; Toxic metals
64

1. Introduction

Dust storms are a severe and worsening global environmental issue (Huang et al., 2014; Huang et al., 2015; Soleimani et al., 2020). The Taklimakan Desert, located in Xinjiang northwest China, re-suspended approximately 70 Tg/yr of mineral dust into the atmosphere over the Spring periods of 2007-2011, making this desert the highest airborne emission source in east Asia (Chen et al., 2017). As an important type of atmospheric aerosol, the dust storm particles can affect climate directly through scattering, transmission and absorption of solar radiation, and indirectly by acting as a cloud nucleation nucleus (CNN) when coated with soluble material (Buseck and Posfai, 1999; Manktelow et al., 2010; Wen et al., 2021; Shi et al., 2005), and can further influence biogeochemical cycles (Li et al., 2017; Uno et al., 2009). Additionally, the smaller respiratory dust particles can cause serious health issues (Hashizume et al., 2020), wheras the coarser particles are nuisance dusts causing nose, throat and eye irritation. It is reported that the aerosol particles can even act as a carrier to spread the Covid-19 virus (Cao et al., 2021). Dust particles can function as carriers of toxic elements and organics (Cave et al., 2018; Li et al., 2013; Tang et al., 2018; Wen et al., 2021) potentially producing free radicals with the resultant production of oxidative stress in the cardiovascular and respiratory systems (Aghababaeian et al., 2021; Chen et al., 2018; Hasunuma et al., 2021; Sadeghimoghaddam et al., 2021).

The compositional characteristics of dust storms depend on two main variables, which are provenance, and the inputs and outputs along the transport route (Li and Shao, 2012; Wang et al., 2022; Zhao et al., 2007). The mineral particles in the dust storms are

87 the most abundant; accounting for more than 80% of all particles (Jeong, 2008; Okada
88 et al., 2005; Wang et al., 2022; Shi et al., 2005). The relative abundances of different
89 minerals, such as clays, calcite, quartz, and feldspars will vary by source region and
90 also by the respective mineral grain's sizes and shapes. The larger mineral grains will
91 be less likely to be suspended in the dust storms and will drop out more rapidly as the
92 storm energy levels decrease. Studies have found that there is a significant difference
93 in the mineralogical composition of dust particles in Asia and Africa, and specifically,
94 the illite/kaolinite ratio and chlorite/kaolinite ratio of Asia dust particles were higher
95 than those of Africa (Formenti et al., 2011). The size, morphology and geochemistry of
96 particles will be modified over the long-distance transport of the storm (Li et al., 2018;
97 Li et al., 2014; Xu et al., 2020). Alkaline minerals, typically containing Ca, Mg, K, Mn
98 and Fe, in the dust can react with acidic atmospheric gases by providing an interface
99 for atmospheric chemical reactions (Fussell and Kelly, 2021; Li and Shao, 2009; Shi et
100 al., 2012; Wang et al., 2017). Over long-range transport, the relative percentages of
101 sulphate, nitrate, and chlorine in the dust particles increase when compared to the
102 original composition (Kim et al., 2012; Ma et al., 2001; Li and Shao, 2012). It is
103 recognised that the relative proportions of sulphate minerals and other compounds
104 change in the dust attenuation stage (Wu et al., 2017), and the total sulphur content in
105 the dust can be lower in the culmination of the storm (Li et al., 2018; Wang et al., 2022).
106 However, the variations in the different forms of sulphur-containing minerals (all
107 minerals containing sulphur) over the duration of the dust storm is unclear.

108 The dust storm events sourced from the Gobi Desert have direct harmful impacts

on the environment and people of north China (Huang et al., 2014; Shao et al., 2008). Beijing experienced three distinct dust storm events in the spring of 2021 (Fig. S1), and one of them started on 15th of March 2021, and was the most widespread in China in the past decade. The dust influence covered an area of 3.8 million square kilometers in China, affecting more than 19 cities (Filonchyk, 2022; Luo et al., 2022b). The data from China National Environmental Monitoring Centre showed that the PM_{10} (particulate matter with mean aerodynamic diameter $\leqslant$10 μm) concentration in six core districts in Beijing reached 8000 μg/m^3 and the $PM_{2.5}$ (particulate matter with mean aerodynamic diameter $\leqslant$2.5 μm) concentration exceeded 400μg/m^3 (China Climate Bulletin, 2021). This very large-scale dust storm provided a significant research opportunity for studying the physical and chemical properties of particulate matter in a highly damaging and impactful event.

In this study, Scanning Electron Microscopy coupled with Energy Dispersive X-ray Spectrometry (SEM-EDX), a commonly used method of individual particle analysis (Shao et al., 2022), was used to analyse the number-size distributions, types, and elemental compositions of individual particles of PM_{10} in Beijing's atmosphere during a dust storm episode. The empirical outputs provide data on particle sizes, numbers, morphologies, elemental compositions, and mixing states, which allows interpretation of the particle's provenance and processes that the particulate matter might have undergone while in the storm. During transport, Asian dust particles can react with anthropogenic acidic species through heterogeneous processes to produce large quantities of water-soluble aerosols (Pan et al., 2017; Tang et al., 2017), influencing the

direct and indirect effects of dust on climate (Wang et al., 2017). Numerous studies have focused on the level of sulphur and the rate of sulphate reactions during dust and sand processes (Li and Shao, 2008; Wang et al., 2022; Wang et al., 2021; Wu et al., 2017). However, there is still uncertainty about the levels of sulphur in dust storms. The results of many studies have shown that during long-distance transport, the dust plumes undergo heterogeneous reactions in the atmosphere, producing large amounts of sulphur-containing particles (Huang et al., 2010; Nie et al., 2012; Zhao et al., 2011). However, other researchers argue that the sulphur content in dust storms is very consistent (Wang et al., 2022; Wu et al., 2017), where the sulphur in dust particles originates from the source area (Hu et al., 2022), and the sulphur content remains virtually unchanged even over long-distance transport (Wu et al., 2017). This study focuses on the variation of sulphur mass concentrations at different stages during a single dust event, providing a reference for the association between dust and atmospheric sulphur.

2. Sampling and Experiments

2.1 Dust sampling

Tracked by satellite remote sensing, the investigated dust storm was initiated in western Mongolia around 15:00 (UTC+8) on the 14th of March 2021, and then crossed into China by the near-border Chinese town of Erenhot and adjacent areas at around 21:00 (UTC+8) on the 14th of March. The dust storm continued to move in a southeasterly direction towards Beijing and arrived in Beijing at around 3:00 (UTC+8)

on the 15th of March. During the dust storm, the highest mass concentration of PM_{10} was recorded on the 15th of March, at a daily mass concentration of 1630 μg/m^3. On the same day, the daily $PM_{2.5}$ mass concentration and the daily AQI value were 207 μg/m^3 and 500, respectively. When the dust storm reached the sampling site in Beijing, the atmospheric pressure, temperature, and relative humidity (RH) were measured and recorded every 30 minutes. These meteorological data were recorded using a portable meteorological tracker (Kestrel 5500 Weather LiNK, USA). The temperature and RH varied from 2.9℃ to 19.5℃ and 9.6% to 90%, respectively. The data for the levels of $PM_{2.5}$, PM_{10}, and AQI in Fig. 1 were derived from the Wanliu state-owned automatic ambient air monitoring station, which was obtained from the downloaded data of each monitoring station in Beijing (https://quotsoft.net/air/). As determined by the levels of PM mass concentration and horizontal visibility (Song et al., 2007), this dust event consisted of three stages, that were initiation, attenuation, culmination. The initiation is on the15th of March with the PM10 mass concentration larger than 3000 μg/m^3 and visibility being less than 500m, the attenuation stage is from the 16th to 17th of March with the daily PM10 mass concentration changing from 200 to 600 μg/m^3 and visibility ranging from 1km to 10km. The culmination stage is from the 19th to 20th of March with the daily PM10 mass concentration being lower than 200 μg/m^3 and visibility being more than 10km.

Airborne particle samples were collected from the 15th of March to the 20th of March 2021. Samples were not collected on the 18th of March due to instrument malfunction. The sampling site was located in the Haidian District, northwest of Beijing,

1 km from the fourth Ring Road. The sampler was placed on the flat roof of a building on the campus of the China University of Mining and Technology (Beijing) (CUMTB). The height of the building roof was 18 m above the ground (Fig. S2). Following the National Standard of Determination of Atmospheric PM_{10} and $PM_{2.5}$ in Ambient Air by Gravimetric Method (HJ 618-2011), the vertical distance between the sampler inlet and the collection surface shall not be less than 1.5 m. The CUMTB campus is surrounded by residential areas and shopping malls. The airborne particles were collected on a polycarbonate (PC; Millipore, UK) filter with apertures of 0.67 μm using a Minivol^{TM} sampler (Airmetrics, USA) with a particle PM_{10} separation device at a flow rate of 5 L/min. The sampling efficiency of the particle separation device is 50% for particles with an aerodynamic diameter of 10 μm.

Since the study was designed to understand the evolution of PM_{10} composition and number-size distribution during the dust storm, eight aerosol samples were collected from the 15th of March to the 20th of March 2021. Two samples were collected in the initiation stage on the 15th of March, four samples in the attenuation stage on the 16th to 17th of March, and two samples in the culmination stage on the 19th to 20th of March. The meteorological data recorded during the sample collections are shown in Table 1.

2.2 Analysis Methods

2.2.1 Electron Microscopy

The particle morphology was imaged using Field Emission Scanning Electron Microscopy (FESEM, SUPRA40, Zeiss, German). The elemental composition of

individual particles was analysed qualitatively and semi-quantitatively by an Oxford Link Pentafet energy spectrum analysis system, which can detect elements heavier than boron (Z＞5). The signal acquisition time varied from 80s to 100s. Each filter was cut into 1 cm^2 and fixed on a cylindrical copper carrier using conductive adhesive. The carrier and sample were gold coated to approximately 20 nm. An area was randomly selected for each sample and more than 300 particles analysed from each filter. Copper and gold were omitted from the analysis.

2.2.2 Image Analysis

To measure the size of every individual particle analysed, the 'area measurement' function of Image-J software was used to process the images taken by SEM. The software draws a line around the perimeter of each particle, then automatically converts the measured length of the perimeter to the geometric Equivalent Spherical Diameter (ESD). A total of 3143 particles were analysed and measured.

3. Results

3.1 Morphologies and chemical compositions of particles during the dust storm

The dust particles showed complex elemental compositions under SEM-EDX. In addition to C and O which were detected in all the particles, N, Na, Mg, Al, Si, P, S, Cl, K, Ca, Ti, Mn, Fe, Zn, and Cr were detected in individual particles (Fig. S3). Si and Al had the highest detection frequency, accounting for 96.0% and 88.4% in the 3143 analyzed particles, respectively, followed by Fe (33.8%), Mg (29.3%), Cl (26.5%), K (21.6%), Ca (19.8%), Mn (15.7%), Na (10.4%), S (4.2%) and Ti (3.9%). Other elements

were present in less than 1%.

The morphologies and elemental compositions from the FESEM-EDX analysis, allows the particles to be classified into three main types recorded during the dust storm, which were minerals, soot, and organic particles (Fig. 2). The minerals are mainly composed of Si and Al, with minor amounts of Na, Mg, and Fe. Minerals that have undergone attrition and abrasion in dust storms are likely to have no recognisable crystalline form (Shi et al., 2005; Shao et al., 2022). The morphologies of the minerals were mainly irregular with a small number of more elongate grains. The minerals were extremely stable under the electron beam. Soot and organic particles were mainly composed of C and O, and could be visually recognised by their characteristic shapes. Soot particles are typically chain-shaped aggregates containing microscopic spherical C nanoparticles. Organic particles were typically spherical or nearly spherical, and were stable under the electron beam.

In the initiation stage on the 15th of March, the proportion of minerals was the highest, accounting for 97.76%. During the attenuation stage of the 16th and 17th of March, the proportion of minerals decreased when compared with the initiation stage, but was still high, accounting for 78.56%. In the culmination stage of the 19th and 20th of March, the percentage of minerals significantly decreased to 55.75%. The percentage of soot continuously increased from the initiation stage to the culmination stage. In the initiation stage, the percentage of soot is only 0.18%, but in the culmination stage, it has increased to 39.83%. The percentage of organic particles remained low throughout the three stages of the dust storm. The relative percentage of organic particles was the

lowest in the initiation stage at only 2.06%. The highest relative percentage of organic particles was during the attenuation stage at 7.04%. Overall, during the whole storm event, the relative number percentage of minerals is the highest, ranging from 47.37% to 99.12%, averaging 77.66%, followed by soot particles, ranging from 0.36% to 46.52%, averaging 17.20%, with organic particles being the least abundant type, ranging from 0.88% to 17.96%, averaging 5.14% (Fig. 3a).

3.2 Classification and characteristics of minerals

Airborne minerals not only affect climate, but also play an important role in atmospheric chemical reactions (Shao et al., 2022; Wang et al., 2021). When transported over a long distance, the dust particles can undergo elemental modifications (Li et al., 2012a). As the total mass of minerals in the dust plume will not be constant due to changing inputs and outputs, then this would change the relative percentages of minerals in that plume. Firstly, the original source minerals could undergo chemical change, with heterogeneous reactions resulting in the formation of different mineral types (Aydin et al., 2012; Wang et al., 2017 and 2022; Yu et al., 2020). Secondly, the mineral composition of the dust mass could change as the original minerals settle out of the cloud, and are replaced with freshly sourced mineral grains (Raffaele et al., 2020). Using the results of the elemental analysis, the formula:

$$P(X) = X / (Na+Mg+Al+Si+S+Cl+K+Ca+Ti+Fe) \times 100\%$$

can be used to divide the mineral particles into different types, where P(X) is the atomic weight ratio of the element (Li and Shao, 2012; Okada et al., 2005; Shao et al., 2017). Through adapting this method and adding Mn and Cr to the formula, a total number of

2343 mineral particles are classified by the formula:

$$P(X) = X / (Na+Mg+Al+Si+S+Cl+K+Ca+Ti+Fe+Mn+Cr) \times 100\%.$$

The minerals were classified as Si-rich, Fe-rich, Ca-rich, Al-rich, Ti-rich, Mg-rich, Mn-rich, Cl-rich and Cr-rich. The minerals containing S are further classified into S-containing minerals (Fig. 3b). In this dust storm event, the most abundant mineral types were Si-rich particles, accounting for 85.51% of the total particles. This was followed by Fe-rich, Ca-rich, and S-containing minerals, accounting for 4.23%, 4.13%, and 4.05% respectively. The Al-rich, Ti-rich, Mg-rich minerals, and other mineral types accounted for 2.37%. The relative number percentage of Si-rich particles decreased over the duration of the dust storm. Fe-rich particles had the highest abundance in the attenuation stage, while Ca-rich particles were the least abundant. The relative number percentage of S-containing minerals increased over the duration of the storm.

There are 8 sub-types of Si-rich particles (Table S1), among which Si + Al particles are the most common. According to their atomic weight ratios of Si and Al, minerals can be categorized into several types of alkaline minerals (Li et al., 2018; Lv and Shao, 2003; Wang et al., 2022). This presents the opportunity to approximate the percentages of common minerals in the dust cloud when the measured data consists only of elemental data, and no mineralogical data such as X-ray diffraction is available. The mineral with a ratio of Si:Al near 1 may be kaolinite, and when Si:Al is between 1 and 2, possible minerals include illite, chlorite, and montmorillonite, in which illite has higher K content, and the value Si:Al of chlorite is closer to 2 (Lv and Shao, 2003; Wang et al., 2022). The Si-rich particles also could consist of potassium feldspar and

plagioclase, which have Si:Al approximately equal to 3, and contain K and Na elements, respectively (Lv and Shao, 2003). Si-dominated particles are mainly quartz, which is dominated by Si and O. Si-rich particles are mainly derived from crustal weathering of silicate minerals and quartz, certainly in the initiation stage. (Fig. S4).

The majority of the Fe-rich particles were identified as hematite, with peaks of Fe and O elements and an absence of other significant components (Fig. S4). The Ca-rich minerals consist mostly of calcite, dolomite and gypsum. The carbonates, calcite and dolomite, were differentiated according to the relative proportions of Ca and Mg (Fig. S4), with dolomite containing a greater proportion of Mg. The third common Ca-containing mineral was identified as gypsum from the amount of S in the spectra; this is important when considering the chemical evolution of S-containing minerals over the duration of the dust storm from initiation to culmination. There was a second common group of S-containing minerals whose more complex composition of Si, Al, S, and other minor elements was interpreted to be a reaction product between silicate minerals and SO_2 (Jeong 2020; Li et al., 2018; Li and Shao, 2012). These S-containing mixtures were discovered throughout the dust storm. In overall, the relative proportion of total S-containing minerals continually increased over the duration of the dust storm; from 1.06% in the initiation to 6.18% in the culmination.

3.3 Number-size distributions of dust particles during the sampling period

The size distribution of airborne particles, as determined by image analysis of SEM images (Fig. 4), is an important parameter to understand the impacts of dust storms, and is related to the reactive surface area, volume, mass, and size. The particle

sizes of all the measured dust samples showed a unimodal distribution with the peak in the 1-2 μm size range. One sample collected on the 19th of March had a peak range of less than 1 μm. It is noted that the collector had a 10 μm cut-off device, however the peak is significantly below this size cut-off. Therefore, the majority of the particles collected were respirable, less than 2.5 μm, and able to be respired deep into the human lung. Clearly given the extremely high total dust load of the storm, much of the mass will have included non-respirable mineral grains acting as a nuisance dust.

The number-size distribution (Zhou et al., 2002) of dust particles during the initiation stage on the 15th of March had a peak in the 1-2 μm size range of approximately 150 dN%/dlog (Dp), and also the smallest size range of the duration of the storm. During the attenuation stage, the16th to 17th of March, the size peak dropped to approximately 120 dN%/dlog (Dp), and the size range slightly increased. Finally, the culmination stage, the 19th of March to the 20th of March had the lowest peak at approximately 100 dN%/dlog (Dp), with those peak particle sizes slightly smaller than the initiation and attenuation stages. In addition, the culmination stage had the largest size range of the three stages. It is conjectured that the secondary reaction particles that formed during the dust transportation and the overall changing nature of the sulphur-containing minerals is evidenced (Fig. 4) by both the chemical SEM-EDX and the relatively smaller secondary particle sizes (Liu et al., 2022; Shao et al., 2021). These results are consistent with previous studies on dust storms and non-dust air pollution periods (Song et al., 2022; Wang et al., 2021; Zhang et al., 2008).

4. Discussion

4.1 Possible sources of the particles during the dust storm period

Previous studies have found that dust storm events in northern China are dominated by minerals, including quartz, clay, feldspar, and carbonates (Formenti et al., 2011; Shao et al., 2008). Studies on the contribution of minerals in dust storms and non-dust periods showed that the number and mass concentrations of airborne mineral particles in Xi'an, Erlianhot, and Zhangbei were higher during the dust storms (Tang et al., 2018; Wu et al., 2017). The NOAA/ARL Hybrid Single-Particle Lagrangian Integrated Trajectory Model (Stein et al., 2015) was employed to calculate the backward trajectories of a dust storm at 500 m elevation that arrived at the Beijing sampling site on the 15th of March and culminated on the 20th of March 2021 (Fig. 5). Fig. 5a shows that the air masses started Mongolia and passed over the deserts of northern China, before reaching Beijing.

The ratios of different chemical elements are widely used to identify dust provenance (Zhao et al., 2007). Therefore the Ca:Al ratio can be employed to identify dust source (Huang et al., 2010; Li et al., 2008; Zhao et al., 2007), and the lower Ca:Al ratio (0.27±0.10~0.73±0.03) is believed to indicate that the dust originated from a northern source (Song et al., 2022). In this study, the Ca:Al during the dust episode ranged from 0.17 to 0.79, which is a similar ratio range to the northern dust. This result is consistent with the identified source from the backward trajectory.

At the dust initiation stage, strong winds suspend crustal mineral particles dominantly Si-rich, from erosion-prone desert surfaces (Fig. 3b). In the following

attenuation stage, soot and organic particles mainly derived from airborne emissions from coal-burning, biomass burning, and vehicle emissions (Li et al., 2016; Shao et al., 2022; Xing et al., 2017) mixed into the dust storm. The relative proportions of the crustal minerals decrease, and anthropogenic particles gradually increase during the storm, indicating that anthropogenic emissions are continuously incorporated into the dust storm. March is part of the 'heating' season in northern China including Beijing, Tianjin, and Hebei, and these urban areas contribute considerable amounts of anthropogenic air pollution to mix into the storms in the attenuation stage (Fig. 5b). The understanding of the relative contributions of local emissions and the distally-sourced mineral particles is essential to fully elucidate the impacts of these significant environmental events (Huang et al., 2010).

Studies on atmospheric chemistry show that reactive gases included in local anthropogenic emissions will modify the composition of dust particles and typically generate sulphates and nitrates (Li and Shao, 2012; Tang et al., 2017; Wu et al., 2017). sulphur-containing mixtures were seen in the initiation stage, which was probably caused by secondary chemical reactions during the dust long-distance transport. The mineral types in the dust storm will be altered constantly as a result of the favorable conditions for heterogeneous chemical reactions and availability of fresh inputs of reactive anthropogenic gasses. Typically, when compared with the common crustal minerals seen in the initiation stage, the altered mineral types in the attenuation stage are more complex in terms of their elemental compositions. In addition, these secondary chemical reactions in the storm will increase the relative number proportions of the

particles with a smaller size range (Shao et al., 2021).

4.2 Variations in elemental compositions in different stages of the dust storm

To elucidate the chemical changes in the dust storm particles during the three stages of initiation, attenuation and culmination, the relative atomic weight percentage of elements was analysed. Fig. 6 shows that the elemental atomic weight percentages of Si, Al, K, and Ti decreased, while Ca, Mg, Fe, Zn, Mn, Cr, and S increased over the three stages; with S being of the most significant change. Typically, Si, Al, K, and Ti are considered to be sourced from mineral dust (Huang et al., 2010; Li et al., 2014; Luo et al., 2022; Shao et al., 2017). Ca and Mg are both sourced from crustal inputs (Huang et al., 2010; Song et al., 2022). Zn, Mn, and Cr are considered to largely originate from anthropogenic sources, such as traffic and industrial emissions (Li et al., 2013; Luo et al., 2022). The atomic weight percentages of heavy metals increase during the attenuation stage supporting the other evidence that anthropogenic emissions are mixed into the dust storm. The very significant increase of sulphur atomic weight percentage shows the important role it plays in the alteration of airborne mineral types. The only feasible source of sulphur in airborne particulate matter is the gas to solid phase change from SO_2 to altered mineral chemistries.

Heavy metals in airborne particulate matter can be harmful to human health (Luo et al., 2022a; Xiao et al., 2013), especially metals such as Zn, Mn and Cr, which showed a significantly positive correlation with DNA oxidative damage (Feng et al., 2020 and 2022). The relative atomic weight of Zn, Mn, and Cr in particles were higher in the attenuation stage than in the initiation stage, and this could be interpreted that the

sampling site was strongly influenced by local air masses in Beijing, Tianjin, and Hebei (Fig. 5). Another comparable study on the enrichment factors of heavy metals in dust particles showed that the increase in Zn and Cr was caused by mixing with local aerosols in the polluted area (Luo et al., 2022).

The types and relative amounts of heavy metals decreased in the culmination stage when compared to the attenuation stage. A previous study suggested that airborne dust masses have the ability to incorporate and remove pre-existing pollutants (Wang et al., 2021). This could mean that metals were taken-up within the dust mass and then physically transported out of the area as the dust storm continued along its trajectory. Anthropogenic airborne metals can only be incorporated into the dust cloud in a solid phase, however once in the cloud they are able to take part in atmospheric chemical reactions (Huang et al., 2010). These reactions could make the heavy metals more or less bioavailable. To properly understand the potential impact of airborne metal-containing particles in dust storms, it is imperative to understand the mass and size distributions of these particles, and whether or not they are respirable. In addition, it is important to know whether the metals are bioavailable once respired into the human lung. This critical information is currently unknown.

4.3 Sulphur chemistry of the dust storm particles

It is believed that heterogeneous sulphur chemical reactions are limited during dust storm events (Wang et al., 2022; Wang et al., 2021; Wu et al., 2017), which can result in a relatively low SO_4^{2-} content in dust particles. However, it has also been recorded that sulphur content during dust days is significantly higher than that during non-dust

417 days (Huang et al., 2010; Li and Shao, 2012; Xu et al., 2017). Typically, gaseous phase
418 sulphur in the atmosphere will undergo oxidative reactions with dust particles, resulting
419 in the formation of sulphate (Sun et al., 2004; Wu et al., 2021). Therefore,
420 anthropogenic SO_2 reacts with the alkaline minerals in the dust storm, forming the new
421 minerals (Jeong, 2020; Li et al., 2018; Wang et al., 2017).

422 SEM showed that the sulphur-containing minerals consist of rod-shaped gypsum
423 (Fig. 7a) and a mixture of sulphur and clay, of which the mixture of sulphur and clay
424 was the most common in the initiation stage. The crystalline shape of rod-shaped
425 gypsum is probably derived from the erosion of the arid surfaces where well-formed
426 crystallinity results from changing water availability, groundwater levels, and sufficient
427 time being available for the growth of recognisable crystals (Garcia-Guinea et al., 2002;
428 Hu et al., 2022). The most well-known source of the minerals with well-formed
429 crystalline shapes are the macroscopic so-called gypsum 'desert roses' or over-lapping
430 crystals commonly called 'swallowtail'; both morphologies can be seen
431 microscopically under SEM (Jones et al., 2001). The mixture of sulphur and clay could
432 be the product of the reaction between alkaline minerals and SO_2 (Jeong, 2020; Li et
433 al., 2018). During the attenuation stage, the observed gypsum crystals tend to be
434 irregular and possess a granulated surface, and commonly are mixed with clay minerals
435 (Fig. 7b, 7c, 7d and 7e) visually identifiable from their platy morphologies. This trend
436 away from well-formed crystallinity continues into the culmination stage (Fig. 7f, 7g,
437 and 7h).

438 The observation of the overall change in particle morphologies supports the

interpretation that there were secondary chemical reactions forming new particle types throughout the dust storm event, with airborne alkaline minerals providing a reaction interface for heterogeneous reactions with SO_2. This speculation was also reinforced by a study of a Beijing dust storm in 2002, which found that the mass percentage of SO_4^{2-} during the dust storm in Beijing was higher than the mass percentage in the Gobi Desert (Zhao et al., 2007). Large amounts of sulphur-containing mixtures were also observed under transmission electron microscopy in samples collected during a dust pollution event during the 4^{th} to 5^{th} of May 2017 and spring of 2015 in Beijing (Li et al., 2018; Wang et al., 2022).

To estimate the change of sulphur concentration over the duration of the dust storm event, the average atomic weight ratio of sulphur in all individual particles was multiplied by the mass concentration of PM_{10} to obtain the mass of atmospheric sulphur as $\mu g/m^3$ (Fig. 8). The mass concentration of sulphur was the highest in the initiation stage, at 27.9 $\mu g/m^3$, and decreased rapidly over the attenuation stage, at 3.7 $\mu g/m^3$. A similar trend was recorded for sulphur in March of 2015 in Beijing, in which mass concentration of sulphur in the dust period are higher than that in the following non-dust period (Wang et al., 2022). In the initiation, gypsum from the source area and sulphur added during transport together contribute to the high concentration of sulphur. The rapid decrease of sulphur concentration in the attenuation stage is a possible consequence of the dust plume sweeping away locally emitted air pollutants (Wang et al., 2021). The mass concentration of sulphur increased in the culmination stage, which was caused by secondary chemical reactions in the atmosphere. It also can be seen from

Fig. 8 that the mass concentration of SO_2 in the atmosphere is lowest during the attenuation stage, and the initiation and culmination stages are similar. During the three dust stages, meteorological conditions varied by 10.07℃, 12.83℃, 11.61℃ for mean temperature, 14.80%, 25.30%, 36.79% for mean relative humidity and 1012.75hPa, 1015.42hPa, 1012.35hPa for mean pressure. The data of meteorological conditions are shown in Table 1. There are no special trends for air temperature and pressure, however, humidity increases from the dust initiation stage to the dust culmination stage. Some other studies have shown a negative correlation between PM_{10} mass concentration and relative humidity (Csavina et al., 2014; Maleki et al. 2022), and a similar trend was found in this dust event. The increase in relative humidity during the dust culmination stage is conducive to the occurrence of sulphate reactions.

A comparison with the mass concentration of sulphur in the 2021 dust storm with a dust event in 2015 showed that the mass concentration of sulphur in the 2021 dust storm period was higher than that seen in 2015 (Fig. 8). This could be due to the difference of source areas and transport pathways. Based on the backward trajectory results, the source area of the 2021 dust storm is northern Mongolia, but the 2015 dust originated in southern Mongolia (Wang et al., 2022). The 2021 dust storm was transported over a longer distance than the 2015 dust storm (Wang et al., 2022). The mass concentration of sulphur in the initiation stage in this study was much higher than that on haze and non-haze days. It is well established that there are large amounts of sulphate particles during haze days due to secondary chemical reactions (Cheng et al., 2016; Li et al., 2022). If we exclude the gypsum particles derived from the source area

in the initiation stage, the calculated sulphur mass concentration (8.26 μg/m^3) was similar to that recorded during the haze periods such as one that occurred in 2017 (11.83 μg/m^3), indicating that secondary chemical reactions were as significant as those during the haze period. The important difference is the presence and impact of the mineral dust particles, and their role as interfaces for sulphates formation and the environmental and adverse human health impacts resulting from dust storms.

5. Conclusions

(1) The dust storms that occurred in Beijing from March 15th to 20th, 2021, consist of three recognisable stages; initiation, attenuation and culmination, with the initiation being associated with the highest PM_{10} mass concentration and lowest horizontal visibility. The dust storm particles can be subdivided into types consisting of minerals, soot, and organic particles identified microscopically. The relative number percentage of minerals continuously decreased, while that of soot and organic particles correspondingly increased. The number-size of particles showed a unimodal distribution with the peak in the 1-2 μm size range during the initiation and attenuation stages, whereas the particles were mainly less than 1 μm in the culmination stage.

(2) Dust plumes consisted of mineral particles from the source area, and later added particles during the transportation. Minerals provide an interface for atmospheric chemical reactions, which leads to the modification of particulate composition and an increase in the types of minerals. The predominant mineral type in the initiation stage was Si-rich particles, followed by Ca-rich, Fe-rich, and Ti-rich particles, with minor amounts of S-containing minerals. During the attenuation and culmination stages, Al-

rich, Mg-rich, and other types of minerals became evident. The relative number percentage of S-containing particles was increasing and the sum of the several remaining mineral particles was decreasing.

(3) The number percentages of metal-containing dust particles were relatively low in the initiation stage, but in the attenuation stage, they increased significantly, demonstrating an increasing trend of anthropogenic emissions mixing into the dust storm. The heavy metals in dust storm particles should be considered because their bioavailability and potential oxidative damage to human health.

(4) Over the duration of the dust storm, the mass concentration of sulphur was highest in the initiation stage, with the main type of sulphur being the crustal mineral gypsum and a mixture of sulphur and clay. The rapid decrease of sulphur concentration in the attenuation stage was caused by the dust plume sweeping away air pollutants. The mass concentration of sulphur-containing mixtures in the initiation stage was similar to that during haze pollution, suggesting that the secondary chemical reactions during dust storm periods were as evident as in haze. In the dust culmination stage, the mass concentration of sulphur slightly increased.

Acknowledgments

This study is supported by the National Natural Science Foundation of China (Grant No. 42075107), the Fundamental Research Funds for the Central Universities, and the Yueqi Scholar fund of China University of Mining and Technology (Beijing).

References

Aghababaeian, H., Ostadtaghizadeh, A., Ardalan, A., Asgary, A., Akbary, M., Yekaninejad, M.S., Stephens, C., 2021. Global health impacts of dust storms: A systematic review. *Environmental health insights 15(*11786302211018390-11786302211018390. 10.1177/11786302211018390.

Aydin, F., Aydin, I., Erdogan, S., Akba, O., Isik, B., Hamamci, C., 2012. Chemical characteristics of settled particles during a dust-storm. *Polish Journal of Environmental Studies 21(3)*, 533-537.

Buseck, P.R., Posfai, M., 1999. Airborne minerals and related aerosol particles: Effects on climate and the environment. *Proceedings of the National Academy of Sciences of the USA 96,* 3372-3379.

Cao, Y.X., Shao, L.Y., Jones, T.J., Oliveira, M.L.S., Ge, S.Y., Feng, X.L., Silva, L.F.O., BéruBé, K.A., 2021, Multiple relationships between aerosol and COVID-19: A framework for global studies. *Gondwana Research* 93, 243-251. https://doi.org/10.1016/j.gr.2021.02.002

Cave, M.R., Wragg, J., Beriro, D.J., Vane, C., Thomas, R., Riding, M., Taylor, C., 2018. An overview of research and development themes in the measurement and occurrences of polyaromatic hydrocarbons in dusts and particulates. *Journal of Hazardous Materials 360,* 373-390.

Chen, Q.C., Wang, M.M., Sun, H.Y., Wang, X., Wang, Y.Q., Li, Y.G., Zhang, L.X., Mu, Z., 2018. Enhanced health risks from exposure to environmentally persistent free radicals and the oxidative stress of PM2.5 from Asian dust storms in Erenhot,

549 Zhangbei and Jinan, China. *Environment International 121*, 260-268.
550 10.1016/j.envint.2018.09.012.
551 Chen, S., Huang, J., Li, J., Jia, R., Jiang, N., Kang, L., Ma, X., Xie, T., 2017.
552 Comparison of dust emissions, transport, and deposition between the Taklimakan
553 Desert and Gobi Desert from 2007 to 2011. *Science China Earth Sciences 60(7)*,
554 1338-1355. 10.1007/s11430-016-9051-0.
555 Cheng, Y.F., Zheng, G.J., Wei, C., Mu, Q., Zheng, B., Wang, Z.B., Gao, M., Zhang, Q.,
556 He, K.B., Carmichael, G., Poschl, U., Su, H., 2016. Reactive nitrogen chemistry
557 in aerosol water as a source of sulfate during haze events in China. *Science*
558 *Advances 2(12)*, ARTN e1601530. 10.1126/sciadv.1601530.
559 China Climate Bulletin, 2021. China Climate Bulletin
560 http://www.cma.gov.cn/zfxxgk/gknr/qxbg/. (Accessed 8 March 2022) (in Chinese).
561 China Meteorological Administration, 2021. China Meteorological Administration.
562 http://www.nmc.cn/publish/environment/National-Bulletin-atmospheric-
563 environment.htm. (in Chinese).
564 Csavina J, Field J, Félix O, Corral-Avitia AY, Eduardo Sáez A, Betterton EA. Effect of
565 wind speed and relative humidity on atmospheric dust concentrations in semi-arid
566 climates. Sci Total Environ. 2014;487:82–90.
567 Feng, X.L., Shao, L.Y., Xi, C.X., Jones, T., Zhang, D.Z., BeruBe, K., 2020. Particle-
568 induced oxidative damage by indoor size-segregated particulate matter from coal-
569 burning homes in the Xuanwei lung cancer epidemic area, Yunnan Province, China.
570 *Chemosphere 256.* 127058-127058. 10.1016/j.chemosphere.2020.127058.

571 Feng, X.L., Shao, L.Y., Jones, T., Li, Y.W., Cao, Y.X., Zhang, M.Y., Ge, S.Y., Yang, C
572 - X., Lu, J., BeruBe, K., 2022. Oxidative potential and water-soluble heavy metals
573 of size-segregated airborne particles in haze and non-haze episodes: Impact of the
574 "Comprehensive Action Plan" in China. *Science of the Total Environment*
575 *814(*152774. 10.1016/j.scitotenv.2021.152774.
576 Filonchyk, M., 2022. Characteristics of the severe March 2021 Gobi Desert dust storm
577 and its impact on air pollution in China. *Chemosphere 287*.
578 10.1016/j.chemosphere.2021.132219.
579 Formenti, P., Schütz, L., Balkanski, Y., Desboeufs, K., Ebert, M., Kandler, K., Petzold,
580 A., Scheuvens, D., Weinbruch, S., Zhang, D., 2011. Recent progress in
581 understanding physical and chemical properties of African and Asian mineral dust.
582 *Atmospheric Chemistry and Physics 11(16)*, 8231-8256. 10.5194/acp-11-8231-
583 2011.
584 Fussell, J.C., Kelly, F.J., 2021. Mechanisms underlying the health effects of desert sand
585 dust. *Environment International 157*. 106790. 10.1016/j.envint.2021.106790.
586 Garcia-Guinea, J., Morales, S., Delgado, A., Recio, C., Calaforra, J.M., 2002.
587 Formation of gigantic gypsum crystals. *Journal of the Geological Society 159*,
588 347-350.
589 Hashizume, M., Kim, Y., Ng, C.F.S., Chung, Y., Madaniyazi, L., Bell, M.L., Guo, Y.L.,
590 Kan, H., Honda, Y., Yi, S.M., Kim, H., Nishiwaki, Y., 2020. Health Effects of
591 Asian Dust: A Systematic Review and Meta-Analysis. *Environmental Health*
592 *Perspectives 128(6)*. 66001. 10.1289/EHP5312.

593 Hasunuma, H., Takeuchi, A., Ono, R., Amimoto, Y., Ha Hwang, Y., Uno, I., Shimizu,
594 A., Nishiwaki, Y., Hashizume, M., Askew, D.J., Odajima, H., 2021. Effect of Asian
595 dust on respiratory symptoms among children with and without asthma, and their
596 sensitivity. *Science of the Total Environment 753 (*ARTN 141585).
597 10.1016/j.scitotenv.2020.141585.
598 Hu, T.F., Wu, F., Song, Y.P., Liu, S.X., Duan, J., Zhu, Y.Q., Cao, J.J., Zhang, D.Z., 2022.
599 Morphology and mineralogical composition of sandblasting dust particles from
600 the Taklimakan Desert. *Science of the Total Environment 834*, 155315.
601 10.1016/j.scitotenv.2022.155315
602 Huang, J.P., Wang, T.H., Wang, W.C., Li, Z.Q., Yan, H.R., 2014. Climate effects of dust
603 aerosols over East Asian arid and semiarid regions. *Journal of Geophysical*
604 *Research-Atmospheres 119(19)*, 11398-11416. 10.1002/2014jd021796.
605 Huang, K., Zhuang, G., Li, J., Wang, Q., Sun, Y., Lin, Y., Fu, J.S., 2010. Mixing of
606 Asian dust with pollution aerosol and the transformation of aerosol components
607 during the dust storm over China in spring 2007. *Journal of Geophysical Research*
608 *115(*10.1029/2009jd013145.
609 Huang, R.J., Cheng, R., Jing, M., Yang, L., Li, Y., Chen, Q., Chen, Y., Yan, J., Lin, C.,
610 Wu, Y., Zhang, R., El Haddad, I., Prevot, A.S.H., O'Dowd, C.D., Cao, J., 2018.
611 Source-specific health risk analysis on particulate trace elements: coal combustion
612 and traffic emission as major contributors in wintertime Beijing. *Environmental*
613 *Science & Technology 52(19)*, 10967-10974. 10.1021/acs.est.8b02091.
614 Huang, Z.W., Huang, J.P., Hayasaka, T., Wang, S.S., Zhou, T., Jin, H.C., 2015. Short-

615 cut transport path for Asian dust directly to the Arctic: a case study. *Environmental*
616 *Research Letters 10(11)*, Artn 114018. 10.1088/1748-9326/10/11/114018.
617 Jeong, G.Y., 2008. Bulk and single-particle mineralogy of Asian dust and a comparison
618 with its source soils. *Journal of Geophysical Research-Atmospheres 113(D2)*, Artn
619 D02208. 10.1029/2007jd008606.
620 Jeong, G.Y., 2020. Mineralogy and geochemistry of Asian dust: dependence on
621 migration path, fractionation, and reactions with polluted air. *Atmospheric*
622 *Chemistry and Physics 20(12)*, 7411-7428.
623 Jones, T.P., Williamson, B.J., BeruBe, K.A., Richards, R.J., 2001. Microscopy and
624 chemistry of particles collected on TEOM filters: Swansea, south Wales, 1998-
625 1999. *Atmospheric Environment 35 (21)*, 3573-3583.
626 Kim, W.H., Song, J.M., Ko, H.J., Kim, J.S., Lee, J.H., Kang, C.H., 2012. Comparison
627 of chemical compositions of size-segregated atmospheric aerosols between Asian
628 dust and non-Asian dust periods at background area of Korea. *Bulletin of the*
629 *Korean Chemical Society 33(11)*, 3651-3656. 10.5012/bkcs.2012.33.11.3651.
630 Li, J., Shao, L.Y., Chang, L.L., Xing, J.P., Wang, W.H., Li, W.J., Zhang, D.Z., 2018.
631 Physicochemical characteristics and possible sources of individual mineral
632 particles in a dust storm episode in Beijing, China. *Atmosphere 9(7)*, ARTN 269.
633 10.3390/atmos9070269.
634 Li, W.J., Shao, L.Y., 2012a. Chemical modification of dust particles during different
635 dust storm episodes. *Aerosol and Air Quality Research 12(6)*, 1095-1104.
636 10.4209/aaqr.2011.11.0188.

637 Li, W.J., Shao, L.Y., Li, Z.P., Li, H., Gao, J., Li, J.J., Zhang, H., Zhang, Z.Z., Silva,
638 L.F.O., Zhang, M.Y., Chen, Y.Z., Oliveira, M.L.S., 2022. Surface chemistry of
639 atmospheric nanoparticles during a haze episode in Beijing by TOF-SIMS.
640 *Gondwana Research 110*, 305-318. 10.1016/j.gr.2022.02.013.
641 Li, W.J., Wang, T., Zhou, S.Z., Lee, S., Huang, Y., Gao, Y., Wang, W.X., 2013.
642 Microscopic observation of metal-containing particles from chinese continental
643 outflow observed from a non-industrial site. *Environmental Science & Technology*
644 *47(16)*, 9124-9131. 10.1021/es400109q.
645 Li, W.J., Shao, L.Y., Shi, Z.B., Chen, J.M., Yang, L.X., Yuan, Q., Yan, C., Zhang, X.Y.,
646 Wang, Y.Q., Sun, J.Y., Zhang, Y.M., Shen, X.J., Wang, Z.F., Wang, W.X., 2014.
647 Mixing state and hygroscopicity of dust and haze particles before leaving Asian
648 continent. *Journal of Geophysical Research-Atmospheres 119(2)*, 1044-1059.
649 10.1002/2013jd021003.
650 Li, W.J., Xu, L., Liu, X.H., Zhang, J.C., Lin, Y.T., Yao, X.H., Gao, H.W., Zhang, D.Z.,
651 Chen, J.M., Wang, W.X., Harrison, R.M., Zhang, X.Y., Shao, L.Y., Fu, P.Q., Nenes,
652 A., Shi, Z.B., 2017. Air pollution-aerosol interactions produce more bioavailable
653 iron for ocean ecosystems. *Science Advance 3(3)*, e1601749.
654 10.1126/sciadv.1601749.
655 Li, W.J., Shao, L.Y., 2009. Observation of nitrate coatings on atmospheric mineral dust
656 particles. *Atmospheric Chemistry and Physics 9*, 1863-1871.
657 Li, W.J., Shao, L.Y., Zhang, D.Z., Ro, C.U., Hu, M., Bi, X.H., Geng, H., Matsuki, A.,
658 Niu, H.Y., Chen, J.M., 2016. A review of single aerosol particle studies in the

atmosphere of East Asia: morphology, mixing state, source, and heterogeneous reactions. *Journal of Cleaner Production 112(*1330-1349. 10.1016/j.jclepro.2015.04.050.

Liu, P.J., Shao, L.Y., Li, Y.W., Wang, W.H., Zhang, M.Y., Yang, C.X., Niu, H.Y., Feng, X.L., Zhang, D.Z., 2022. Compositions, sources, and aging processes of aerosol particles during winter hazes in an inland megacity of NW China. *Atmosphere 13 (4)*, ARTN 521. 10.3390/atmos13040521.

Luo, H., Wang, Q., Guan, Q., Ma, Y., Ni, F., Yang, E., Zhang, J., 2022a. Heavy metal pollution levels, source apportionment and risk assessment in dust storms in key cities in Northwest China. *Journal of Hazardous Materials 422(*126878. 10.1016/j.jhazmat.2021.126878.

Luo, J., Huang, F., Gao, S., Liu, S., Liu, R., Devasthale, A., 2022b. Satellite monitoring of the dust storm over Northern China on 15 March 2021. *Atmosphere 13(2)*, 10.3390/atmos13020157.

Lv, S.L., Shao, L.Y., 2003. Mineral compositions of individual particulates in PM10 over Beijing. *ACTA Petrologica et Mineralogica 22(4)*, 421-424. DOI: 10.3969/j.issn.1000-6524.2003.04.023. (in Chinese with English abstract)

Ma, C.J., Kasahara, M., Holler, R., Kamiya, T., 2001. Characteristics of single particles sampled in Japan during the Asian dust-storm period. *Atmospheric Environment 35(15)*, 2707-2714. Doi 10.1016/S1352-2310(00)00410-6.

Maleki, H., Sorooshian, A., Alam, K., Fathi, A., Weckwerth, T., Moazed, H., Jamshidi, A., Babaei, A.A., Hamid, V., Soltani, F., Goudarzi, G., 2022. The impact of

meteorological parameters on PM10 and visibility during the Middle Eastern dust storms. *Journal of Environmental Health Science and Engineering* 10.1007/s40201-022-00795-110.1007/s40201-022-00795-1.

Manktelow, P.T., Carslaw, K.S., Mann, G.W., Spracklen, D.V., 2010. The impact of dust on sulfate aerosol, CN and CCN during an East Asian dust storm. *Atmospheric Chemistry and Physics 10(2)*, 365-382. 10.5194/acp-10-365-2010.

Nie, W., Wang, T., Xue, L. K., Ding, A. J., Wang, X. F., Gao, X. M., Xu, Z., Yu, Y. C., Yuan, C., Zhou, Z. S., Gao, R., Liu, X. H., Wang, Y., Fan, S. J., Poon, S., Zhang, Q. Z., Wang, W. X., Asian dust storm observed at a rural mountain site in southern China: chemical evolution and heterogeneous photochemistry, Atmos. Chem. Phys., 12, 11985–11995, https://doi.org/10.5194/acp-12-11985-2012, 2012.

Okada, K., Qin, Y., Kai, K., 2005. Elemental composition and mixing properties of atmospheric mineral particles collected in Hohhot, China. *Atmospheric Research 73(1-2)*, 45-67. 10.1016/j.atmosres.2004.08.001.

Pan, X.L., Uno, I., Wang, Z., Nishizawa, T., Sugimoto, N., Yamamoto, S., Kobayashi, H., Sun, Y.L., Fu, P.Q., Tang, X., Wang, Z.F., 2017. Real-time observational evidence of changing Asian dust morphology with the mixing of heavy anthropogenic pollution. *Scientific Reports 7 (ARTN 335)*.10.1038/s41598-017-00444-w.

Raffaele, L., Bruno, L., Sherman, D.J., 2020. Statistical characterization of sedimentation velocity of natural particles. *Aeolian Research 44*. 10.1016/j.aeolia.2020.100593.

703 Shao, L.Y., Hu, Y., Fan, J., Wang, J., Wang, J., Ma, J., 2017. Physicochemical
704 characteristics of aerosol particles in the Tibetan Plateau: Insights from TEM-EDX
705 analysis. *Journal of Nanoscience and Nanotechnology 17(9)*, 6899-6908.
706 10.1166/jnn.2017.14472.
707 Shao, L.Y., Li, J., Zhang, M.Y., Wang, X., Li, Y.W., Jones, T., Feng, X.L., Silva, L.F.O.,
708 Li, W.J., 2021. Morphology, composition and mixing state of individual airborne
709 particles: Effects of the 2017 Action Plan in Beijing, China. *Journal of Cleaner*
710 *Production 329.* 10.1016/j.jclepro.2021.129748.
711 Shao, L.Y., Liu, P.J., Jones, T., Yang, S.S., Wang, W.H., Zhang, D.Z., Li, Y.W., Yang,
712 C.-X., Xing, J.P., Hou, C., Zhang, M.Y., Feng, X.L., Li, W.J., BéruBé, K., 2022. A
713 review of atmospheric individual particle analyses: Methodologies and
714 applications in environmental research. *Gondwana*
715 *Research* .10.1016/j.gr.2022.01.007.
716 Shao, L.Y., Li, W.J., Xiao, Z.H., Sun, Z.Q., 2008. The mineralogy and possible sources
717 of spring dust particles over Beijing. *Advances in Atmospheric Sciences 25,* 395-
718 403.
719 Shi, Z.B., Shao, L.Y., Jones, T.P., Lu, S.L., 2005. Microscopy and mineralogy of
720 airborne particles collected during severe dust storm episodes in Beijing, China.
721 *Journal of Geophysical Research 110* (d1), pp. 1-10.
722 Soleimani, Z., Teymouri, P., Boloorani, A.D., Mesdaghinia, A., Middleton, N., Griffin,
723 D.W., 2020. An overview of bioaerosol load and health impacts associated with
724 dust storms: A focus on the Middle East. *Atmospheric Environment 223*(ARTN

117187). 10.1016/j.atmosenv.2019.117187.

Song, L.L., Bi, X.H., Zhang, Z.Y., Li, L.X., Dai, Q.L., Zhang, W.H., Li, H., Wang, X.H., Liang, D.N., Feng, Y.C., 2022. Impact of sand and dust storms on the atmospheric environment and its source in Tianjin-China. *Science of the Total Environment 825(*10.1016/j.scitotenv.2022.153980.

Song, Z.X., Wang, J.Y., Wang, S.G., 2007. Quantitative classification of northeast Asian dust events. *Journal of Geophysical Research 112*. 10.1029 /2006JD007048.

Stein, A.F., Draxler, R.R., Rolph, G.D., Stunder, B.J.B., Cohen, M.D., Ngan, F., 2015. Noaa's hysplit atmospheric transport and dispersion modeling system. *Bulletin of the American Meteorological Society 96(12)*, 2059-2077. 10.1175/Bams-D-14-00110.1.

Sun, Y.L., Zhuang, G.S., Yuan, H., Zhang, X.Y., Guo, J.H., 2004. Characteristics and sources of 2002 super dust storm in Beijing. *Chinese Science Bulletin 49(7)*, 698-705. 10.1360/03wb0157.

Tang, K., Huang, Z.W., Huang, J.P., Maki, T., Zhang, S., Shimizu, A., Ma, X.J., Shi, J.S., Bi, J.R., Zhou, T., Wang, G.Y., Zhang, L., 2018. Characterization of atmospheric bioaerosols along the transport pathway of Asian dust during the Dust-Bioaerosol 2016 Campaign. *Atmospheric Chemistry and Physics 18(10)*, 7131-7148. 10.5194/acp-18-7131-2018.

Tang, M.J., Huang, X., Lu, K.D., Ge, M.F., Li, Y.J., Cheng, P., Zhu, T., Ding, A.J., Zhang, Y.H., Gligorovski, S., Song, W., Ding, X., Bi, X.H., Wang, X.M., 2017. Heterogeneous reactions of mineral dust aerosol: implications for tropospheric

747 oxidation capacity. *Atmospheric Chemistry and Physics 17(19)*, 11727-11777.
748 10.5194/acp-17-11727-2017.
749 Uno, I., Eguchi, K., Yumimoto, K., Takemura, T., Shimizu, A., Uematsu, M., Liu, Z.Y.,
750 Wang, Z.F., Hara, Y., Sugimoto, N., 2009. Asian dust transported one full circuit
751 around the globe. *Nature Geoscience 2(8)*, 557-560. 10.1038/Ngeo583.
752 Wang, W.H., Shao, L.Y, Zhang, D.Z., Li, Y.W., Li, W.J., Liu, P.J., Xing, J.P., 2022.
753 Mineralogical similarities and differences of dust storm particles at Beijing from
754 deserts in the north and northwest. *Science of the Total Environment 803*(149980).
755 10.1016/j.scitotenv.2021.149980.
756 Wang, W.H., Shao, L.Y., Guo, M.L., Hou, C., Xing, J.P., Wu, F., 2017. Physicochemical
757 properties of individual airborne particles in Beijing during pollution periods.
758 *Aerosol and Air Quality Research 17(12)*, 3209-3219.
759 Wang, Z., Hu, W., Niu, H., Hu, W., Wu, Y., Wu, L., Ren, L., Deng, J., Guo, S., Wu, Z.,
760 Zhang, D., Fu, P., Hu, M., 2021. Variations in physicochemical properties of
761 airborne particles during a heavy haze-to-dust episode in Beijing. *Science of the*
762 *Total Environment 762*, 10.1016/j.scitotenv.2020.143081.
763 Wang, Z., Pan, X.L., Uno, I., Chen, X.S., Yamamoto, S., Zheng, H.T., Li, J., Wang,
764 Z.F., 2018. Importance of mineral dust and anthropogenic pollutants mixing
765 during a long-lasting high PM event over East Asia. *Environmental Pollution 234*
766 368-378. 10.1016/j.envpol.2017.11.068.
767 Wen, H., Zhou, Y., Xu, X.Y., Wang, T.S., Chen, Q.L., Chen, Q.C., Li, W.J., Wang, Z.,
768 Huang, Z.W., Zhou, T., Shi, J.S., Bi, J.R., Ji, M.X., Wang, X., 2021. Water-soluble

769 brown carbon in atmospheric aerosols along the transport pathway of Asian dust:
770 Optical properties, chemical compositions, and potential sources. *Science of the*
771 *Total Environment 789*, 10.1016/j.scitotenv.2021.147971.
772 Wu, F., Zhang, D.Z., Cao, J.J., Guo, X., Xia, Y., Zhang, T., Lu, H., Cheng, Y., 2017.
773 Limited production of sulfate and nitrate on front-associated dust storm particles
774 moving from desert to distant populated areas in northwestern China. *Atmospheric*
775 *Chemistry and Physics 17(23)*, 14473-14484. 10.5194/acp-17-14473-2017.
776 Wu, Z.X., Hu, T.F., Hu, W., Shao, L.Y., Sun, Y.Z., Xue, F.L., Niu, H.Y., 2022. Evolution
777 in physicochemical properties of fine particles emitted from residential coal
778 combustion based on chamber experiment. *Gondwana Research 110*, 252-263.
779 10.1016/j.gr.2021.10.017.
780 Xiao, Z.H., Shao, L.Y., Zhang, N., Wang, J., Wang, J.Y., 2013. Heavy metal
781 compositions and bioreactivity of airborne PM10 in a valley-shaped city in
782 Northwestern China. *Aerosol and Air Quality Research 13(3)*, 1116-1125.
783 10.4209/aaqr.2012.10.0287.
784 Xing, J.P., Shao, L.Y., Zheng, R., Peng, J.F., Wang, W.H., Guo, Q., Wang, Y.H., Qin,
785 Y.H., Shuai, S.J., Hu, M., 2017. Individual particles emitted from gasoline engines:
786 Impact of engine types, engine loads and fuel components. *Journal of Cleaner*
787 *Production 149*, 461-471. https://doi.org/10.1016/j.jclepro.2017.02.056.
788 Xu, L., Fukushima, S., Sobanska, S., Murata, K., Naganuma, A., Liu, L., Wang, Y.Y.,
789 Niu, H.Y., Shi, Z.B., Kojima, T., Zhang, D.Z., Li, W.J., 2020. Tracing the evolution
790 of morphology and mixing state of soot particles along with the movement of an

Asian dust storm. *Atmospheric Chemistry and Physics 20(22)*, 14321-14332. 10.5194/acp-20-14321-2020.

Xu, P., Zhang, J.K., Ji, D.S., Liu, Z.R., Tang, G.Q., Hu, B., Jiang, C.S., Wang, Y.S., 2017. Evaluating the effects of springtime dust storms over beijing and the associated characteristics of sub-micron aerosol. *Aerosol and Air Quality Research 17(3)*, 680-692. 10.4209/aaqr.2016.05.0195.

Yu, Z., Jang, M., Kim, S., Bae, C., Koo, B., Beardsley, R., Park, J., Chang, L.S., Lee, H.C., Lim, Y.-K., Cho, J.H., 2020. Simulating the impact of long-range-transported Asian mineral dust on the formation of sulfate and nitrate during the KORUS-AQ campaign. *ACS Earth and Space Chemistry 4 (7)*, 1039–1049.

Zhang, R., Han, Z.W., Shen, Z.X., Cao, J., 2008. Continuous measurement of number concentrations and elemental composition of aerosol particles for a dust storm event in Beijing. *Advances in Atmospheric Sciences 25(1)*, 89-95. 10.1007/s00376-008-0089-2.

Zhao, J., Zhang, F., Xu, Y., Chen, J., Yin, L., Shang, X., Xu, L., Chemical characteristics of particulate matter during a heavy dust episode in a coastal city, Xiamen, 2010, Aerosol Air Qual. Res., 11, 299–308, https://doi.org/10.4209/aaqr.2010.09.0073, 2011.

Zhao, X.J., Zhuang, G.S., Wang, Z.F., Sun, Y.L., Wang, Y., Yuan, H., 2007. Variation of sources and mixing mechanism of mineral dust with pollution aerosol - revealed by the two peaks of a super dust storm in Beijing. *Atmospheric Research 84(3),* 265-279. 10.1016/j.atmosres.2006.08.005.

Zhou, J.C., Swietlicki, E., Hansson, H.C., Artaxo, P., 2002. Submicrometer aerosol particle size distribution and hygroscopic growth measured in the Amazon rain forest during the wet season. *Journal of Geophysical Research-Atmospheres 107* (D20),

Figures and Tables:

Figures:

Tables:

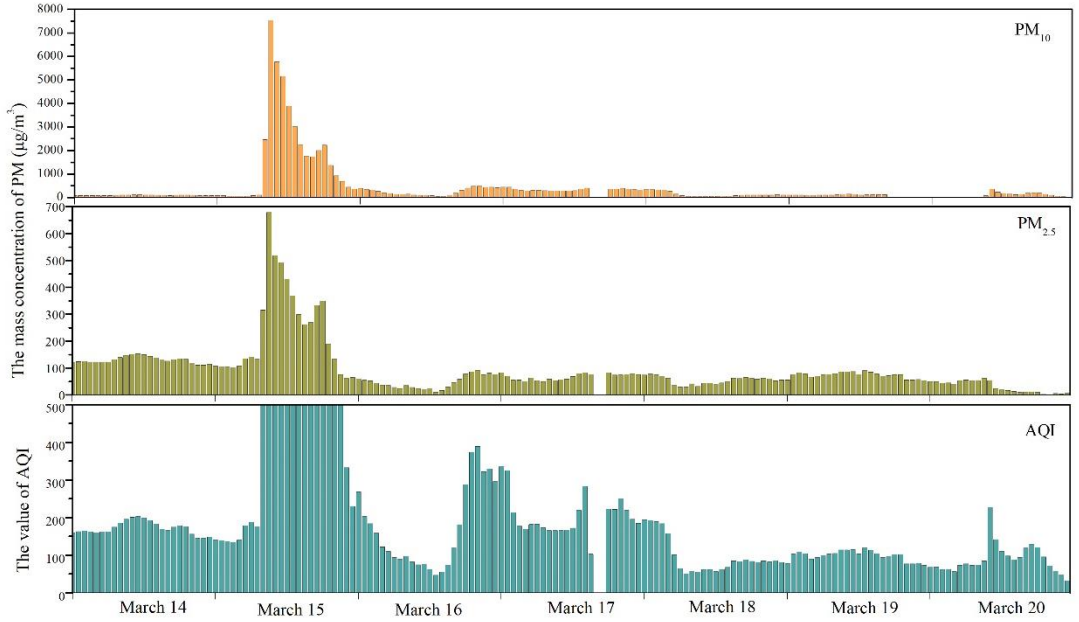

Fig. 1. The hourly mass concentrations of PM10 and PM2.5 and the value of air quality index (AQI) in dust episode

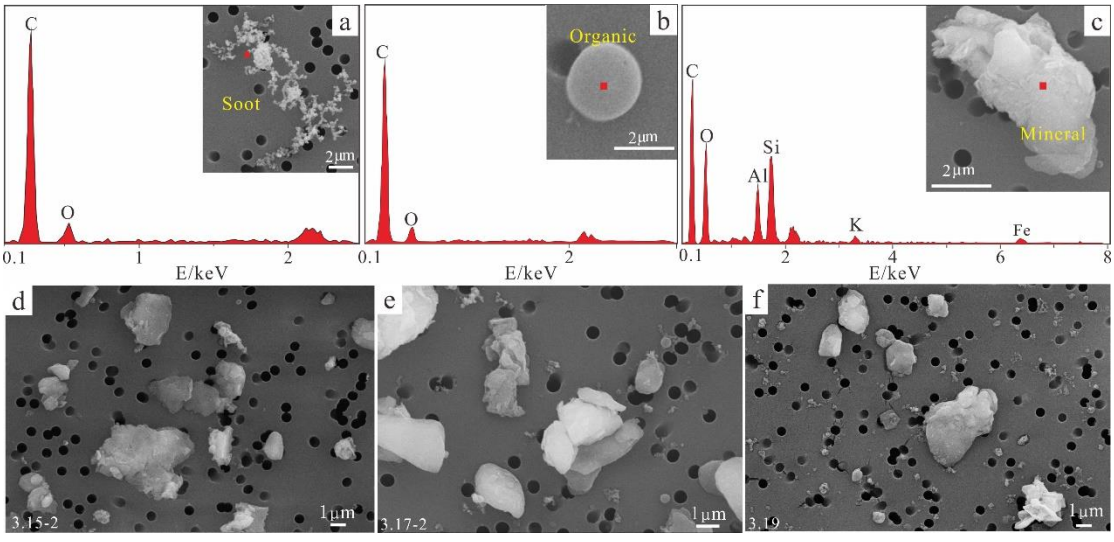

Fig. 2. Morphology and elemental composition of different particle types during dust pollution. (a) soot is mainly composed of C and O, whose morphology is mainly a chain aggregate being composed of carbon spheres from Sample 3.16-2; (b) organic particles are also composed of C and O and the SEM image showed spherical or nearly spherical particles from Sample 3.17-1; (c) mineral particles are mainly composed of Si and Al,

with a small amount of K, Fe. and their morphologies are mainly irregular shape from Sample 3.17-1; (d) the sample collected in the dust initiation stage, when the mineral particles were the dominant. Sample 3.15-2 (number percentage of mineral particles is 97.76%); (e) the sample collected in the dust attenuation stage. The relative number percentage of mineral particles was lower than that in dust initiation stage. Samples 3.17-2 (number percentage of mineral particles is 78.56%, with minor organic particles); (f) the samples collected in the dust culmination stage, with obviously lowered number percentage of minerals. Samples 3.19 (number percentage of mineral particles is 55.75%).

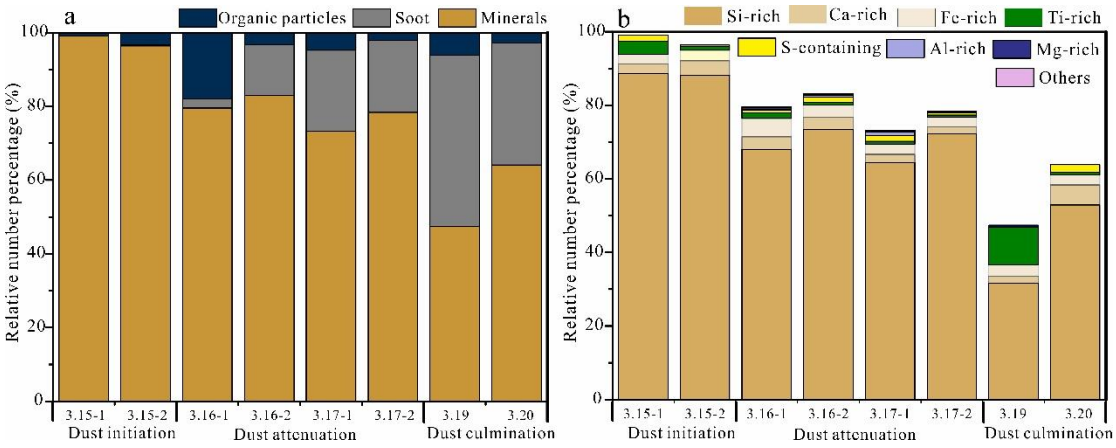

Fig. 3. The relative number percentage of individual particles in PM_{10} during the dust sampling period. (a) refers to the relative proportions of mineral, soot and organic particles in the total analysed particles. (b) refers to the relative proportions of different types of mineral particles in the various pollution stages.

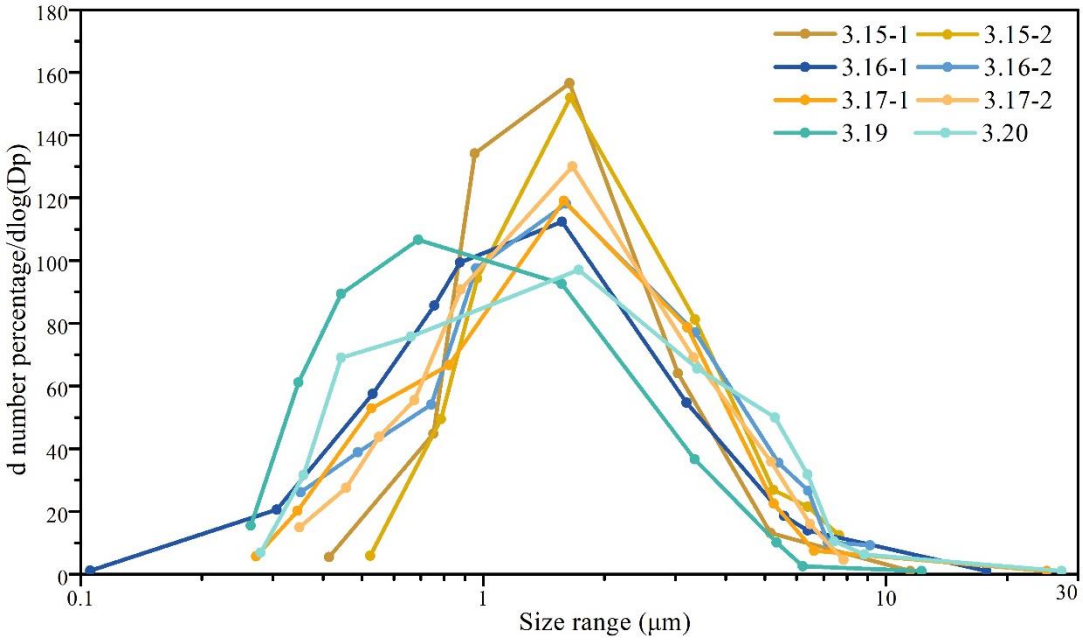

Fig. 4. Number percentage-size distribution of dust particle in PM_{10}. In the 1-2 μm size range, the number of individual particles in the dust storm period (3.15) was highest and the number in 3.17 was higher than that in 3.16, indicating that dust mass carried the coarse particles. In less than 1 μm size range, the number of particles was highest in non-dust period, followed by that in 3.17, which suggested that secondary reactions product the smaller particles

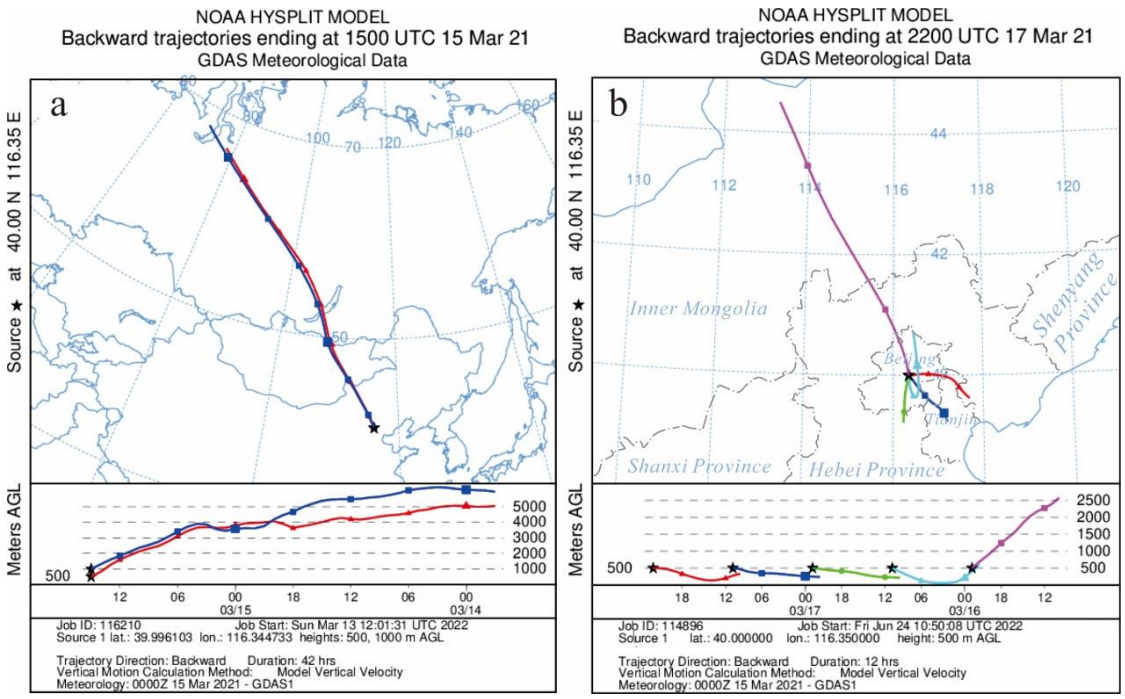

Fig. 5. Air mass backward trajectories from March 15 to March 18, 2021, at the sampling site in Beijing

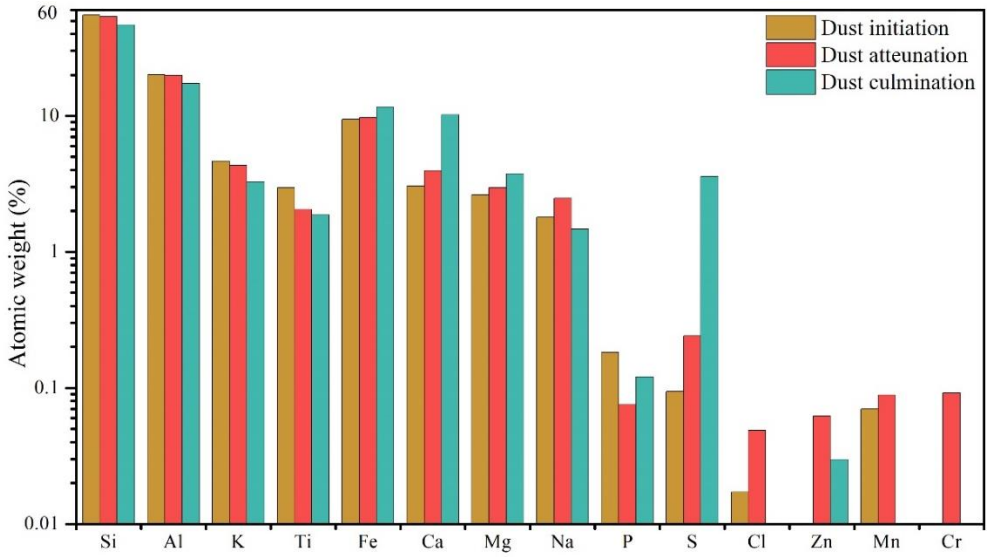

Fig. 6. Atomic weight ratio of elements in PM_{10} during different dust pollution stages. The elemental atomic weight radios of Si, Al, K, and Ti were decreasing during the dust storm. Fe, Ca, and Mg were increasing during the dust storm. Zn, Mn, and Cr were least in the dust initiation stage. S was increasing in the dust storm.

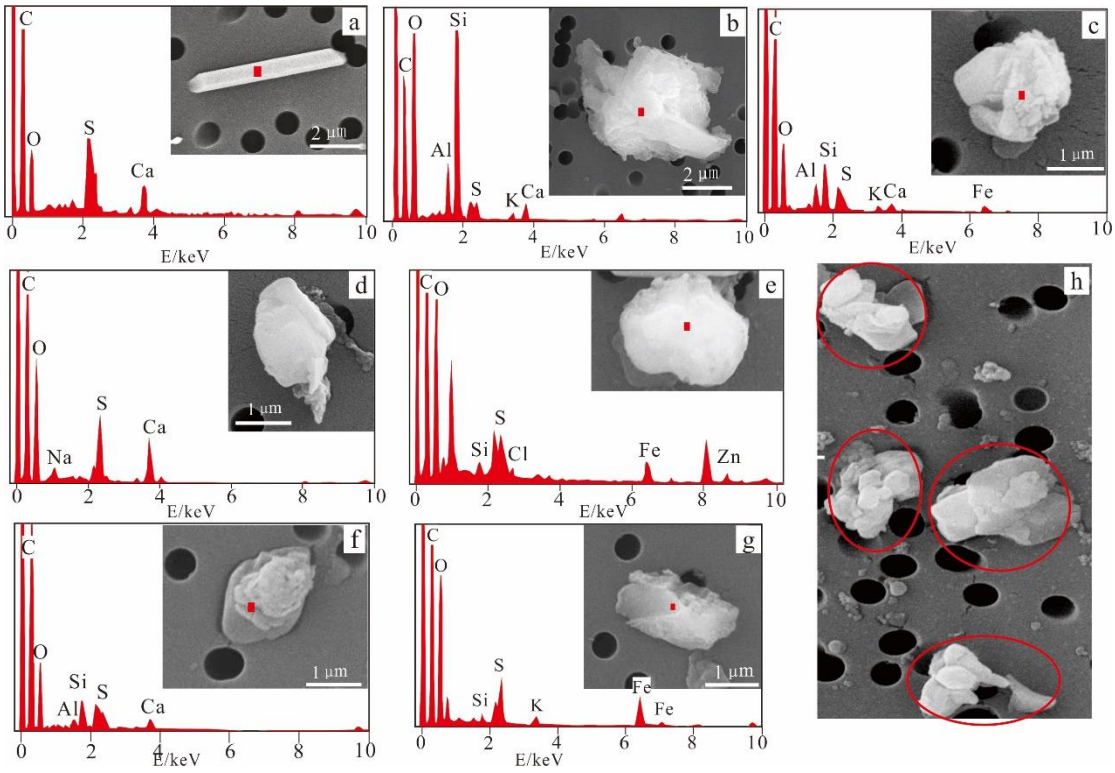

Fig. 7. SEM images and elemental compositions o of S-containing minerals. (a) Rod-shaped gypsum collected in March 15; (b) clay mineral with a small amount of S collected in March 16; (c) the mixture of S and clay mineral collected in March 17; (d) irregular gypsum and (e) the mixture of S and clay minerals, both collected in March 16; (f) gypsum attached in clay mineral and (g) S attached in clay mineral collected in March 20; (h) the mixture of S and clay mineral collected on March 19

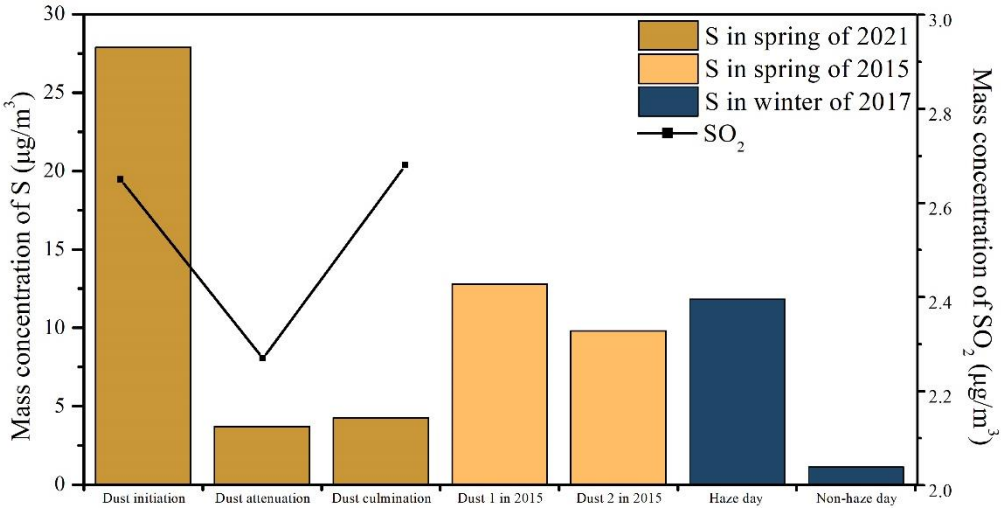

Fig. 8. Mass concentration of S in different dust storm stages and haze pollution in Beijing. Data for the dust storm of 2015 were from Wang et al. (2022) and data for the haze and non-haze days of 2017 were from Shao et al., (2021).

Table 1 Sampling periods and meteorological parameters during the dust episodes

	Sampling ID	Sampling Period, Beijing time	Meteorological Parameters		
			T (℃)	RH (%)	P (hPa)
Dust initiation	3.15-1	15:30-17:30	11.16	13.94	1010.80
	3.15-2	21:00-2:00	8.98	15.65	1014.70
Dust attenuation	3.16-1	8:40-12:10	13.16	13.03	1017.94
	3.16-2	20:30-2:30	12.26	22.86	1013.85
	3.17-1	8:30-12:30	13.14	36.16	1015.44
	3.17-2	15:13-19:00	12.75	29.13	1014.44
Dust culmination	3.19	10:40-16:40	11.42	47.28	1012.51
	3.20	9:30-21:30	11.80	26.29	1012.18

Beijing time: UTC plus 8 hours, T: temperature, RH: relative humidity, P: pressure.

Supplement material

Figures and Tables:

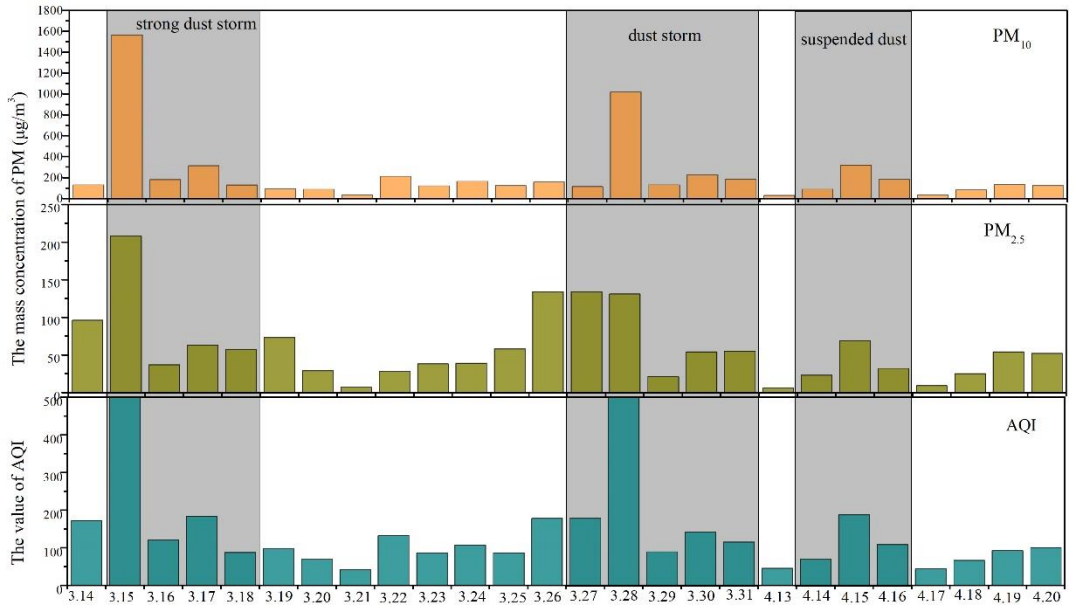

Fig. S1 The daily mass concentrations of PM_{10} and $PM_{2.5}$ and the value of air quality index (AQI) in in Beijing in spring 2021. The value of AQI and PM came from China National Environmental Monitoring Centre (http://www.cnemc.cn/). The dust pollution data came from China Meteorological Administration (China Meteorological Administration, 2021).

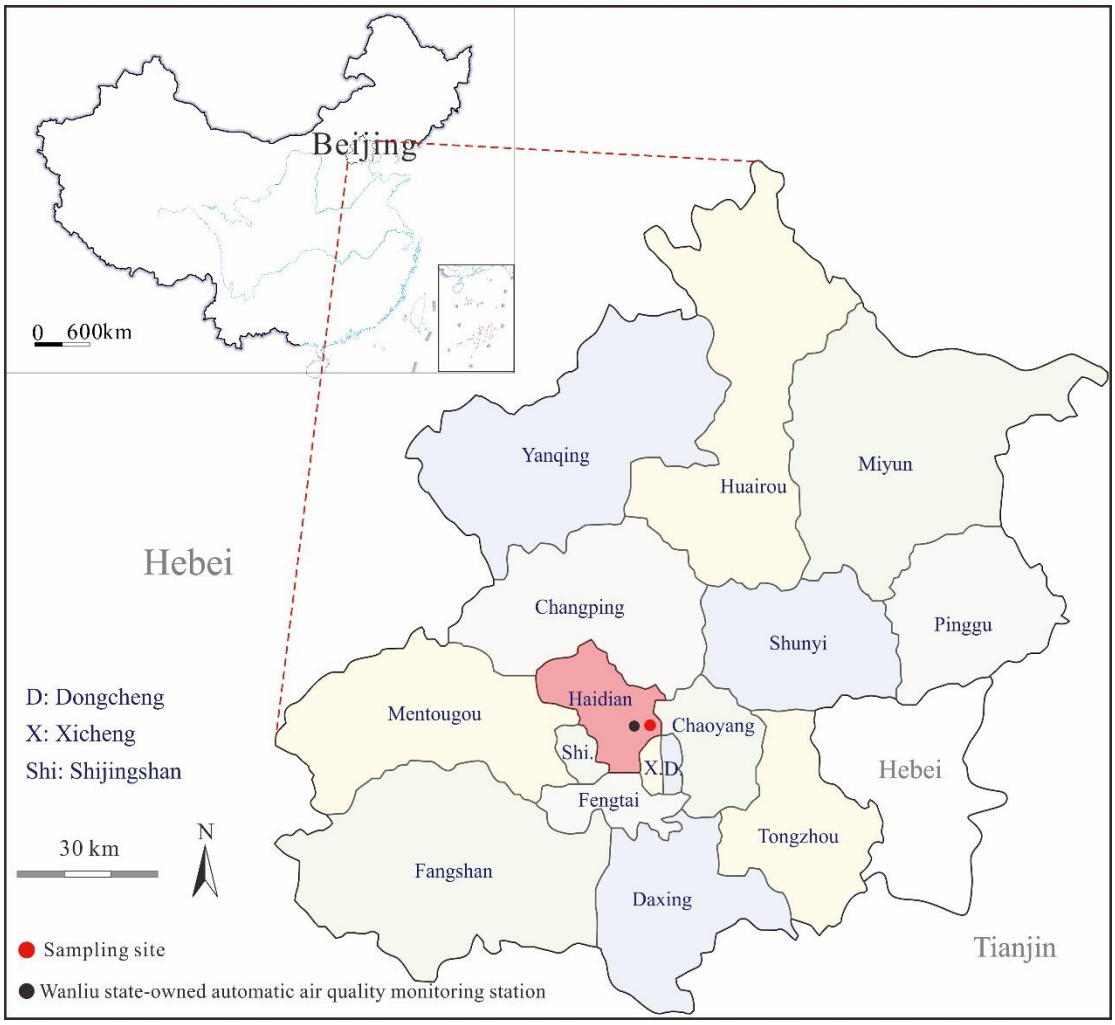

Fig. S2 The distribution map of Wanliu state-owned automatic air quality monitoring station and sampling site

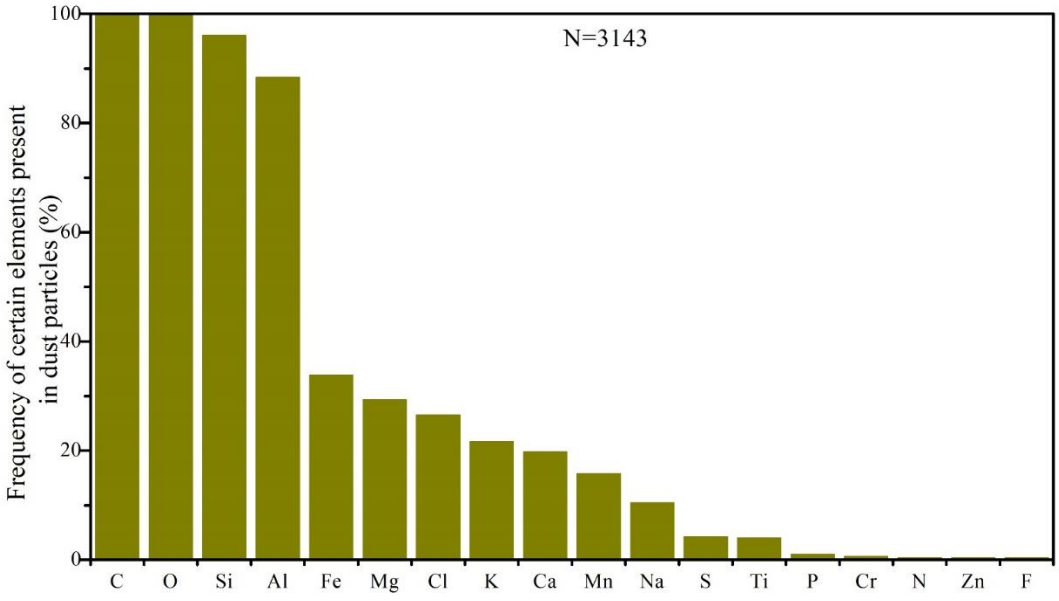

Fig. S3 Overall detection frequencies of elements in dust particles

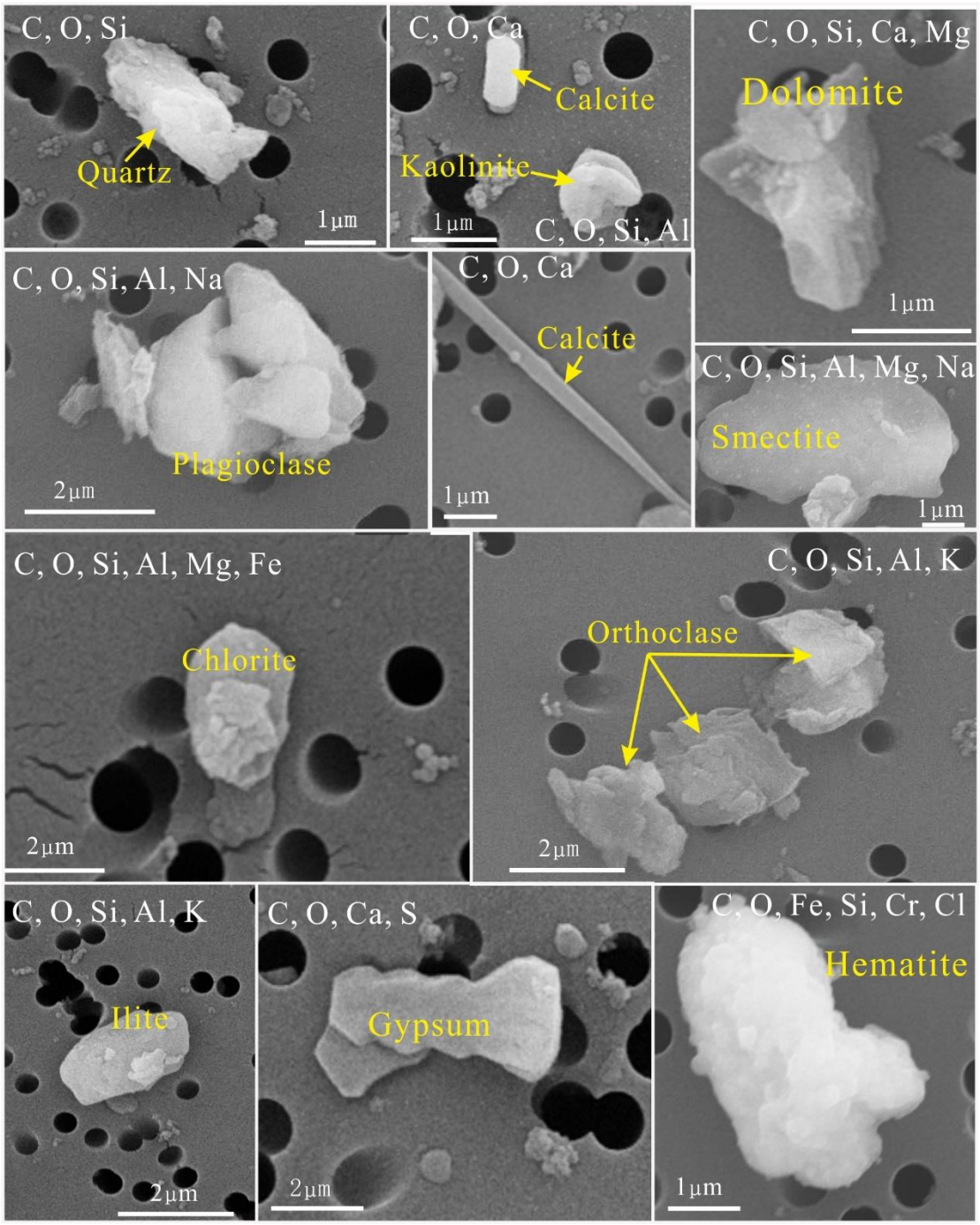

Fig. S4 The different types of mineral particles in dust pollution

Table S1 The number of mineral particles in different dust pollution stages

	Ca-rich				Fe-rich			Ti-rich		Al-rich		Mg-rich	
	Ca-dominated	Ca+Mg	Ca+Si	Other	Fe-dominated	Fe+Si	Other	Ti-dominated	Ti+Si	Al-dominated	Al+Si	Mg-dominated	Mg+Si
Dust initiation	4	2	7	1	7	4		5	2				
Dust attenuation	21	8	10	1	21	24	5	11	2	4	4	3	1
Dust culmination	22	5	1	1	12	11	4	2		1	3		

	Si-rich								S-containing	others
	Si-dominated	Si+Al	Si+Fe	Si+Ca	Si+Na	Si+Mg	Si+K	Other		
Dust initiation	89	219	20	6	3	1	6	2	3	
Dust attenuation	253	645	62	8	34	2	25	3	16	2

Dust culmination	96	204	30	11	6	8	5	67